RSC Advances

PAPER

View Article Online
View Journal | View Issue

Cite this: *RSC Adv.*, 2026, **16**, 21423

Controlled immobilization of single-domain antibodies using cellulose-binding modules for AB_5-type toxin detection in paper-based assays

Selma B. Belfakir, *[ab] Jonas A. Jürgensen, [a] Marcus Petersson, [d] Max Stæhr Wraae,[d] Patrick Munk, [c] Suthimon Thumtecho, [be] Mateus G. Masteghin, [f] Anne Ljungars, [b] Andreas H. Laustsen, [abd] Sandra W. Thrane [d] and Georgina M. S. Ross *[a]

The rapid and sensitive detection of toxigenic *Vibrio cholerae* and enterotoxigenic *Escherichia coli* remains a critical challenge for effective disease screening and environmental monitoring, which is essential for guiding clinical management and outbreak control in regions where diarrheal diseases are endemic. To address this, we developed a single-domain antibody (V_HH)-based sandwich-format lateral flow assay for the rapid and sensitive detection of cholera toxin from *V. cholerae* and heat-labile enterotoxin from enterotoxigenic *Escherichia coli* in human fecal and environmental water samples. It can be challenging to directly immobilize small proteins such as V_HHs onto nitrocellulose while controlling their orientation to support optimal binding. To overcome this challenge, a bifunctional fusion protein comprising a V_HH and a cellulose-binding module (CBM) was developed, enabling controlled orientation and immobilization of the V_HH on nitrocellulose membranes. Using this fusion protein as the test line in an LFA allowed for the capture of cholera toxin and heat-labile enterotoxin across a wide dynamic working range (1–1000 ng mL^{-1}), with detection limits down to 12.5 ng mL^{-1} in human fecal samples and 1 ng mL^{-1} in water. The findings presented here highlight the potential of using a CBM to facilitate the immobilization of a V_HH in a sandwich format lateral flow assay for the rapid and sensitive detection of bacterial toxins in complex matrices.

Received 6th February 2026
Accepted 31st March 2026

DOI: 10.1039/d6ra01063f

rsc.li/rsc-advances

1. Introduction

Diarrheal diseases caused by bacteria that produce AB_5-type toxins, such as cholera toxin (CTX) from *Vibrio cholerae* or the heat-labile enterotoxin (LT) from enterotoxigenic *Escherichia coli* (ETEC), remain a leading cause of reduced quality of life, morbidity, and mortality in low- and middle-income countries (LMICs).[1,2] These diseases are driven by inadequate access to safe drinking water, in addition to poor sanitation and hygiene practices, and are primarily spread *via* the fecal-oral route through contaminated food or water. Following ingestion, ETEC or toxigenic *V. cholerae* strains secrete toxins (LT or CTX, among others), which attach to the monosialotetrahexosylganglioside (GM1 ganglioside) receptor on intestinal epithelial cells through a pentameric B subunit (LT-B or CTX-B).[1] After binding to GM1, the toxin is endocytosed, initiating an intracellular cyclic adenosine monophosphate (cAMP)-driven cascade that ultimately causes watery diarrhea and vomiting that can rapidly lead to severe dehydration.[1] Although manageable with oral rehydration solutions and antibiotics in severe cases, ETEC and cholera-mediated diarrhea remain a leading cause of morbidity and mortality in LMICs.[1,2] Particularly, cholera is still regarded as a major public health concern across Africa, Asia, and Central and South America, with the ongoing seventh cholera pandemic continuing to expand and causing several million cases and more than a hundred thousand deaths worldwide each year.[2] Similarly, ETEC causes an estimated 220 million cases per year, significantly contributing to the global diarrheal disease burden.[3,4] Due to the similar toxin-driven virulence, *V. cholerae* and ETEC infections are diarrheal diseases with overlapping clinical symptoms.[5] In this context, it is relevant to note that the toxin subunits, CTX-B and LT-B, share approximately 80% identity at the amino acid level,[5] which highlights an opportunity for the development of integrated diagnostic approaches that detect the causative agent of these diseases.[6]

Typically, detection of ETEC and/or *V. cholerae* in the clinic relies on bacterial culture. Although this method is specific and inexpensive, it is slow (about 24 hours) and depends on

[a]*VenomAid Diagnostics ApS, DK-2800 Kongens Lyngby, Denmark. E-mail: gin@venomaid.com*

[b]*Department of Biotechnology and Biomedicine, Technical University of Denmark, DK-2800 Kongens Lyngby, Denmark. E-mail: selbel@dtu.dk*

[c]*National Food Institute, Technical University of Denmark, DK-2800 Kongens Lyngby, Denmark*

[d]*Bactolife A/S, DK-2100 Copenhagen, Denmark*

[e]*Division of Toxicology, Department of Medicine, Chulalongkorn University, King Chulalongkorn Memorial Hospital, The Thai Red Cross Society, Bangkok, Thailand*

[f]*DTU Nanolab, Technical University of Denmark, DK-2800 Kongens Lyngby, Denmark*

laboratory infrastructure, limiting its use in many endemic regions.[7] For *V. cholerae*, commercial tests are available that detect the presence of the bacterium, but their specificity and sensitivity are variable.[8] An overview of the tests available for the detection of ETEC and *V. cholerae* can be seen in Table S1. Rapid tests detecting bacteria can be negatively impacted by cross-contamination, lytic bacteriophages, or antibiotics, leading to false results.[9,10] Such false results can lead to unnecessary public health responses, as occurred in South Africa, where a suspected *V. cholerae* outbreak was ultimately traced back to a laboratory contamination.[9,10] Another option well-suited to simultaneously screening many targets is metagenomics. However, this method has low sensitivity, requires deep and expensive sequencing, and downstream computation. For example, the metagenomic assemblies that revealed that non-toxigenic *V. cholerae* persisted in Copenhagen sewage cost thousands of USD and took several weeks to complete, making this method inappropriate for rapid screening.[11] Currently, the gold standard for detecting ETEC infections is based on the polymerase chain reaction (PCR) technology. While sensitive, PCR is slow and often unavailable in endemic regions due to the need for specialized laboratories.[12]

Rapid and sensitive detection of toxigenic bacteria that cause diarrheal disease, such as *V. cholerae* and ETEC, is essential for appropriate clinical management and for guiding timely health responses.[1,13] Recently, the Global Task Force on Cholera Control (GTFCC) published a Target Product Profile (TPP) pointing towards integrating CTX detection for optimal disease monitoring.[14] In line with this, there is a growing need for rapid tests for bacterial pathogens that detect the primary causative agent responsible for the main pathology of the clinical disease. This approach offers the potential for improved specificity and the ability to detect cases where culture conditions are unfavourable.[13] Compared to DNA-based methods, such as quantitative PCR (qPCR) or metagenomics, toxin detection measures the phenotype directly, showing that both transcription and translation of virulence factors have occurred.

Lateral flow assays (LFAs) are potential candidates for rapid, low-cost, detection of pathogenic bacteria as they fulfill the criteria of affordability (<3 USD) highlighted in the GTFCC's TPP, and can conform to the World Health Organization's (RE)ASSURED criteria (real-time connectivity, ease of specimen collection and environmental friendliness, affordable, sensitive, specific, user-friendly, rapid, equipment-free, delivered) that guides disease control strategies and define benchmark standards for point-of-care (POC) diagnostics.[15] Currently, two commercially available LFAs have been approved by the GTFCC for cholera detection, but both target bacterial surface antigens, which prevents them from discriminating between toxigenic and non-toxigenic strains.[16–20] In contrast, at the time of writing, no rapid tests are commercially available for the detection of ETEC, although some have been described in the literature, as summarized in Table S1.

Despite their benefits, LFAs also have drawbacks as they often lack the sensitivity and specificity of other laboratory-based methods.[21] However, it should be recognized that on-site screening assays such as LFAs have different performance requirements than laboratory-based methods, and it is not strictly necessary for on-site methods to achieve the same level of performance as their laboratory counterparts. With the emergence of novel antibody formats with unique functions, such as single-domain antibodies (*e.g.*, V_HHs), there is an opportunity to implement these as immunoreagents to improve the performance of LFAs and allow the detection of targets that could be challenging to reach with full-length antibodies.[22–27] Single-domain antibodies offer several advantages over conventional immunoglobulin G (IgG), including their small size, allowing them to reach cryptic epitopes, high stability, and efficient recombinant expression and genetic engineering.[23,24] Furthermore, their small size can allow for a denser coating onto assay membranes, increasing the number of available binding sites for capturing the target toxin, without compromising affinity.[23] However, their small size also makes it challenging to immobilize V_HHs in an oriented manner on nitrocellulose membranes. Previous studies have demonstrated that cellulose-binding modules (CBMs), protein domains with high affinity for cellulose, can be genetically fused to V_HHs to enable their direct immobilization onto cellulose-based materials.[28,29] Crucially, CBMs can be fused to V_HHs distal to their binding site, allowing V_HHs to be immobilized in an optimal orientation for interacting with their target.

In this work, we have developed a sandwich-format LFA using an engineered bifunctional fusion protein consisting of a V_HH with specificity towards both CTX and LT (anti-CTX/LT V_HH)[30] genetically fused to a CBM as the test line. The assay, which works in 15 minutes, has a wide dynamic working range with the ability to detect CTX and LT down to concentrations of 12.5 ng mL^{-1} in fecal samples and 1 ng mL^{-1} in water samples. These findings demonstrate the promising nature of leveraging CBMs to immobilize V_HHs in LFAs for the rapid and precise detection of bacterial toxins in complex samples to support current diarrheal disease management practices.

2. Materials & methods

2.1. Matrix samples

Human fecal samples were purchased from Innovative Research (USA) and Medix Biochemica (USA) (see Table S2 for a detailed overview of the samples). Prior to testing, fecal samples were diluted 1 : 1 in Milli-Q (MQ) water (>18.2 MΩ cm^{-1}) from Millipore (Burlington, USA) and vortexed to mimic diarrhea consistency. Tap water was collected directly from the tap (Kongens Lyngby, Denmark; Cinque Terre and Pisa, Italy; Casablanca and Marrakech, Morocco; Amsterdam and Utrecht, The Netherlands; Bali, Indonesia; Boston, The United States of America).

2.2. Toxins

For testing the LFA, all B-subunits, CTX-B, LT-B, and Shiga toxin (STX) B-subunit were recombinantly expressed using *E. coli*,[31] LT was expressed using the prototypical human ETEC strain H10407 and consequently purified,[31] and CTX was purchased (Sigma-Aldrich, C8052).

2.3. V_HH–CBM expression and purification

The anti-CTX/LT V_HH (LT109)[30,31] was cloned into the pSANG10-3F expression vector together with the sequence of either CBM_{Cel6A}

(CBM1) or CBM_{Cel7A} (CBM2)[32] and genetically fused with a $(GGGGS)_3$ linker. The anti-CTX/LT V_HH–CBM1 or anti-CTX/LT V_HH–CBM2 constructs were transformed into *E. coli* BL21 (DE3) and incubated overnight while shaking at 220 rpm in lysogeny broth supplemented with 50 μg mL^{-1} kanamycin at 30 °C. 100 μL of the overnight culture was used to inoculate 100 mL of auto-induction medium, which was incubated for 72 hours at 30 °C while shaking at 150 rpm. Cells were centrifuged at 4300 g for 30 min and the supernatant discarded, before resuspension in 5 mL g^{-1} of cell pellet in TES (30 mM Tris–HCl pH 8.0, 1 mM EDTA, 20% sucrose (w/v)) supplemented with 1 tablet per 50 mL of cOmplete Protease Inhibitor Cocktail (Roche, 11697498001), 1.5 mg g^{-1} of cell pellet lysozyme (Sigma-Aldrich, 62971), and 100 U DNase 1 (AppliChem, A3778) per 10 mL of TES. The resuspended cell pellet was vortexed and incubated at 30 °C while shaking at 150 rpm for 30 min. Milli-Q water was added at a 1 : 1 (v/v) ratio, incubated on ice for 10 min, then centrifuged at 20 000 g for 30 min at 4 °C. Purification was performed by immobilized metal affinity chromatography (IMAC) using gravity-flow columns (Bio-Rad, 7321010). HisPur Ni-NTA resin (Thermo Scientific, 10038124) was added to the supernatant at 50 mg mL^{-1} and incubated at 4 °C and 150 rpm for 30 min. The resin-supernatant mixture was added to chromatography columns. The columns were washed twice with IMAC wash buffer (Phosphate-Buffered Saline (PBS) with 200 mM NaCl and 20 mM imidazole). Then, IMAC elution buffer (PBS with 200 mM NaCl and 250 mM imidazole) was added to the column, and the anti-CTX/LT V_HH–CBM1 and anti-CTX/LT V_HH–CBM2 were collected. Protein concentration was determined by a spectrophotometer (Thermo Scientific, NanoDrop One) at 280 nm.

2.4. V_HH expression and purification

The anti-CTX/LT V_HH was expressed in *K. phaffii*. First, a −80 °C glycerol stock was inoculated in 20 mL BMGY media in a 50 mL tube and incubated overnight at 30 °C while shaking at 160 rpm. The overnight culture was diluted to an OD_{600} of 1 in 100 mL BMY media supplemented with 2% glucose and incubated overnight at 30 °C and 160 rpm, after which 20 mL of 5 M NaOH per liter of culture was added, and the mixture was centrifuged at 15 000 g for 15 min. The supernatant was filtered through a 0.2 μm filter. Purification was performed by IMAC using gravity-flow columns. HisPur Ni-NTA resin was added to the supernatant at 50 mg mL^{-1} and incubated at 4 °C and 150 rpm for 30 min. The resin-supernatant mixture was added to chromatography columns and washed with IMAC wash buffer, followed by a final wash with IMAC wash buffer. The protein was eluted with IMAC elution buffer, dialyzed overnight at 4 °C against PBS using dialysis tubing with a 3.5 kDa molecular weight cut-off, and concentrated to approximately 1 mL using a centrifugal concentrator. Protein concentration was determined using a spectrophotometer at 280 nm.

2.5. Circular dichroism spectroscopic analysis of recombinant proteins

The secondary structures of the antigen (CTX-B) and the V_HHs (anti-CTX/LT and anti-CTX/LT–CBM1) were examined using circular dichroism (CD) spectroscopy as previously described.[33] Far-Ultra Violet (UV) CD measurements were conducted using a JASCO J-1500 spectrophotometer (Easton, US) equipped with a 0.1 mm quartz cuvette. The spectra were recorded by performing 10 measurements between 250 nm and 190 nm, with a bandwidth of 0.1 nm, intervals of 1 nm, and a scan speed of 50 nm $minute^{-1}$.

The acquired spectra were processed and smoothed using SpectraManager software (JASCO), and graphs depicting the CD spectra were generated using GraphPad Prism 10.

2.6. Chemical coupling to gold nanoparticles

50 μg anti-CTX/LT V_HH and 50 μg mouse IgG (Sigma-Aldrich, 1003399526, USA) were chemically coupled to 40 nm carboxyl-coated gold nanoparticles (AuNPs) at OD 20 (NanoComposix, USA) according to the manufacturer's protocol (Protocol S1).[28]

2.7. Ultraviolet-visible spectroscopy of gold nanoparticle-conjugated V_HHs

Anti-CTX/LT V_HH–AuNP and mouse IgG-AuNP coupling was confirmed by ultraviolet-visible (UV-vis) spectroscopy (Shimadzu UV-1280 spectrophotometer). Milli-Q water and the conjugate diluent were used as blanks prior to loading the bare AuNPs and V_HH–AuNP conjugates, respectively. Absorbance spectra were measured from 400 to 800 nm and normalized to the peak maximum. Conjugation was inferred by monitoring the red-shift in the localized surface plasmon resonance (LSPR) peak (λ_{max}) of the AuNPs.[34]

2.8. Scanning transmission electron microscopy characterization of gold nanoparticle-conjugated V_HHs

A control sample (gold nanoparticles, AuNP), conjugated AuNP (anti-CTX/LT V_HH–AuNP) and conjugated AuNP in the presence of antigen (anti-CTX/LT V_HH–AuNP + CTX-B) were imaged *via* scanning transmission electron microscopy (STEM). In brief, the samples were prepared by diluting 2 μL of AuNP, anti-CTX/LT V_HH–AuNP or an anti-CTX/LT V_HH–AuNP-antigen mix (2 μL anti-CTX/LT-AuNP with 10 μL of 10 000 ng mL^{-1} CTX-B) in 98 μL of ultrapure water. Lacey carbon-coated copper grids (Agar Scientific) were glow-discharged for 10 seconds (current: 10 mA, air: 3.0×10^{-1}) using EM ACE600 (Leica Microsystem). 3 μL of the prepared samples were drop-casted onto the glow-discharged grids and incubated for 2 minutes before excess was blotted off with filter paper. Following, 5 μL of uranyl acetate was spotted onto the grid and incubated for 1 minute, excess was removed by blotting, and the grids were washed with 5 μL MilliQ water. STEM was carried out in a Talos F200X G2 (Thermo Fisher Scientific) using a 70 mm C2 aperture and "spot-size" 5, resulting in a probe current <100 pA and a convergence semi-angle of 10.5 mrad. Images were acquired using high-angle annular dark-field, bright-field, and dark-field detectors. Bright-field TEM was performed to confirm the crystal structure of the AuNP.

2.9. Lateral flow assay fabrication

LFAs were developed on backed nitrocellulose membrane cards (HF135NC; flow rate of 135 s/4 cm, Millipore, Merck, Germany). Two glass-fiber conjugate pads (Millipore, Merck, Germany) were used with a 2 mm overlap. One conjugate pad contained mouse IgG-AuNP diluted 1 : 1 in conjugate pad buffer (5 mM borate buffer (BB) (pH 8.8), containing 100 mM sodium tetraborate, 100 mM boric acid (Sigma-Aldrich, Switzerland) with 5% or 10% sucrose (Sigma-Aldrich, USA)) and dispensed at 10 μL cm^{-1}, and the second conjugate pad contained anti-CTX/LT V_HH–AuNP diluted 1 : 1 in conjugate pad buffer and dispensed at 20 μL cm^{-1}. Both conjugates were dispensed using the μAirjet of the XYLite BioDot platform (Irvine, USA). A 20 mm sample pad (Millipore, Merck, Germany) was added below the conjugate pads with an overlap, and a 40 mm absorbent pad (Whatman, GE Healthcare, Germany) was affixed to the opposite end of the nitrocellulose membrane with an overlap. Test and control line reagents were diluted in 5 mM BB, 1% D(+)-trehalose dihydrate (w/v) (Carl Roth GmbH, Germany) and 1% ethanol (VWR Chemicals, France) before dispensing (conditions: 1 μL cm^{-1} at a rate of 20 mm s^{-1}) using the BioDot platform. The LFAs had 0.25 mg mL^{-1} of goat anti-mouse $F(ab')_2$ (Jackson Immunoresearch, UK) as a control line and 1.5 mg mL^{-1} or 2 mg mL^{-1} anti-CTX/LT V_HH–CBM as the test line. After dispensing, LFAs were dried for one hour at room temperature, cut to 4 mm with a CM5000™ Guillotine Cutter (BioDot, USA), and stored at room temperature in heat-sealed foil bags with desiccant pouches until use. A schematic representation of the developed LFA can be seen in Fig. 1.

2.10. Examination of immobilization of anti-CTX/LT V_HH–CBM

Ponceau S (Thermo Scientific, USA) staining was used to examine the immobilization of anti-CTX/LT V_HH–CBM1 onto nitrocellulose in two different immobilization buffers (5 mM BB with 1% trehalose or 5 mM PBS (Gibco, UK) with 1% trehalose (w/v)), according to the method previously described.[28,35]

2.11. Determining the optimal running condition for the lateral flow assay

An overview of the experiments is provided in Table S3. In the following experiments, the antigen (CTX-B or LT-B) was diluted to the desired concentration in running buffer (RB), which consisted of PBS with 0.3% Tween-20. All tests were left to develop for 15 minutes.

First, a comparison was made between LFAs with either 1.5 mg mL^{-1} anti-CTX/LT V_HH–CBM1 or 1.5 mg mL^{-1} anti-CTX/

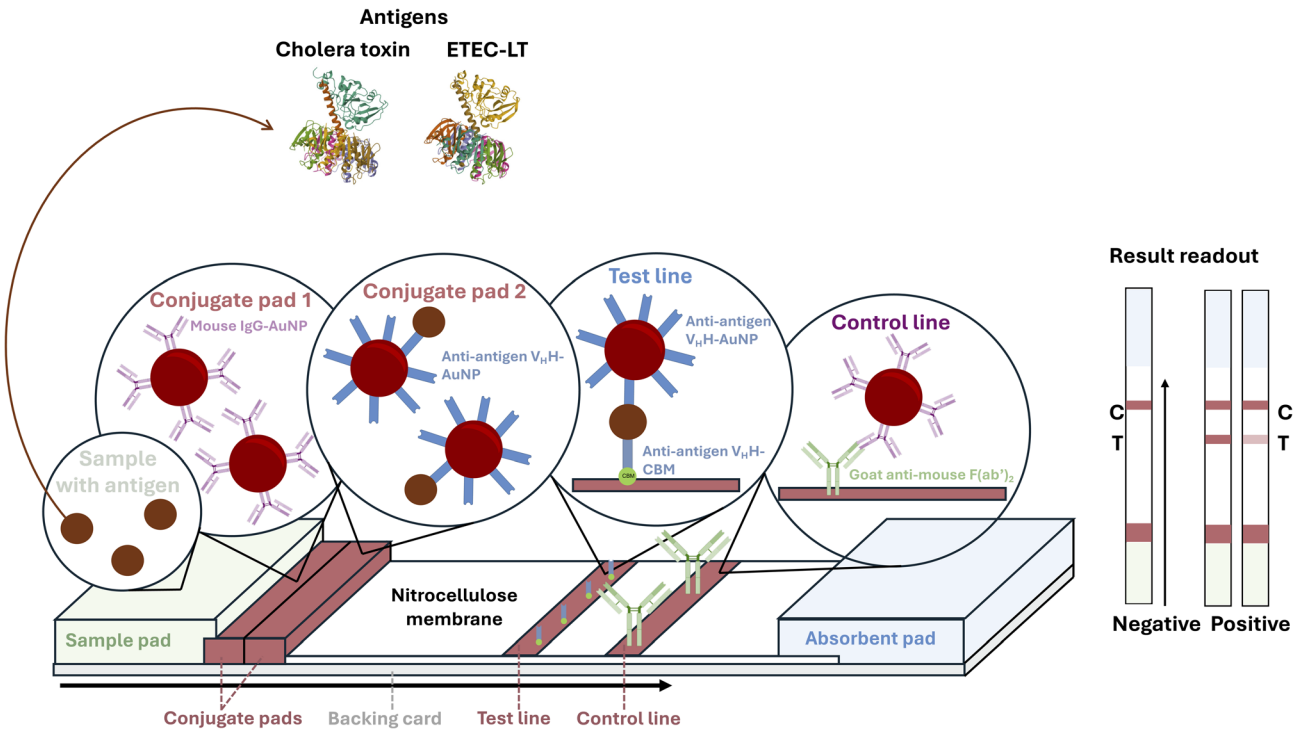

Fig. 1 Schematic representation of the lateral flow assay architecture. A sample containing antigen (cholera toxin or *E. coli* heat-labile enterotoxin (ETEC-LT)) is added to the sample pad and moves up the strip by capillary action. Conjugate pad 1 contains mouse immunoglobulin G (IgG) chemically coupled to gold nanoparticles (AuNPs), and conjugate pad 2 contains anti-antigen single-domain antibodies (V_HHs) chemically conjugated to AuNPs. When the sample reaches the conjugate pads, the conjugates are released. When reaching conjugate pad 2, the antigens will bind to the anti-antigen V_HH–AuNP. When this complex then reaches the test line, a sandwich pair is formed between the anti-antigen V_HH–AuNP and the immobilized anti-antigen V_HH–cellulose-binding module (CBM) with the antigen in between. Thereafter, when the sample reaches the control line, the mouse IgG-AuNP from conjugate pad 1 will bind to an immobilized goat anti-mouse $F(ab')_2$. Finally, the remaining sample is absorbed by the absorbent pad. A negative test is represented by a single line at the control region, and a positive test is represented by a line at the control and test regions. Antigen structures are adapted from ref. 37 and 38.

LT V_HH–CBM2 as the test line (no control line) by inserting the LFAs ($n = 2$) into a microwell containing 20 μL of CTX-B (0, 100, or 1000 ng mL^{-1}), 80 μL of RB (PBS with 0.3% Tween-20), and 2 μL anti-CTX/LT V_HH–AuNP. Next, test line concentration was assessed by testing the LFA with the preferred V_HH–CBM at two concentrations (1.5 and 2 mg mL^{-1}) and CTX-B (0, 100, 1000, 10 000 ng mL^{-1}) using the same assay conditions as described above.

After establishing the most appropriate CBM and concentration, a comparison was made between an LFA with a test line of 2 mg mL^{-1} V_HH directly immobilized by passive adsorption (LFA 1) and an LFA with a test line consisting of 2 mg mL^{-1} V_HH–CBM (LFA 2). The LFAs were run ($n = 2$) by inserting the LFAs into a microwell containing 20 μL of CTX-B or LT-B (0, 1, 10, 100, 1000 ng mL^{-1}), 80 μL of RB (PBS with 0.3% Tween-20), and 2 μL anti-CTX/LT V_HH–AuNP.

Thereafter, the optimal RB was selected using the 2 mg mL^{-1} test line LFA in RBs containing PBS with 0%, 0.1%, 0.2%, or 0.3% Tween-20. Furthermore, three different AuNP (anti-CTX/LT V_HH–AuNP) volumes were tested: 2 μL, 3 μL, and 4 μL. Conjugate pad buffers containing (i) 5 mM BB pH 8.8 with 5% sucrose, (ii) PBS pH 7.4 with 5% sucrose, (iii) conjugate diluent (0.5% PBS with 0.5% Bovine Serum Albumin (BSA) (Protease and IgG-free, Jackson Immunoresearch, UK), 0.5% casein (Carl Roth GmBH + Co. KG, Germany), 1% Tween-20 (Sigma-Aldrich, USA), and 0.05% sodium azide (Ampliqon, Denmark)) or (iv) the undiluted gold AuNPs directly sprayed onto the conjugate pad, were compared. For these experiments, the LFA was tested in blank RB or RB spiked with CTX-B (10 000 ng mL^{-1}).

Lastly, using the same conditions as established above, LFAs were tested in a total volume of 100 μL with 1%, 5%, 10%, and 20% fecal sample (sample #1) spiked with CTX-B (10 ng mL^{-1}) in RB.

Two concentrations (0.5 mg mL^{-1} and 1 mg mL^{-1}) of anti-alpaca IgG (V_HH domain) were diluted in 5 mM borate buffer containing 1% trehalose and spotted as a control line on a nitrocellulose membrane. LFAs ($n = 2$) were tested in a blank sample containing 100 μL RB and 2 μL anti-CTX/LT V_HH–AuNP.

Using the optimal conditions chosen above, the LFA (test line: 2 mg mL^{-1} anti-CTX/LT V_HH–CBM1, control line: 0.25 mg mL^{-1} goat anti-mouse $F(ab')_2$ specific) was tested ($n = 3$) in 5 μL sample (RB or fecal sample) spiked with CTX-B or LT-B and 95 μL RB (PBS with 0.3% Tween-20). When spiked into RB, CTX-B and LT-B were tested at 0, 1, 10, 100, 1000, 10 000, or 100 000 ng mL^{-1}, and when spiked into fecal samples, CTX-B and LT-B were tested at 0, 1, 10, 100, or 1000 ng mL^{-1}.

2.12. Optimization of LFA for fecal samples and determination of the limit of detection

The RB was further optimized by inserting LFAs ($n = 2$) into wells containing 5 μL of blank or CTX-B (100 ng mL^{-1}) spiked human fecal sample (sample #1) and 95 μL RB (PBS with 0.3% Tween-20 with or without 0.5% BSA), and the test was allowed to develop for 15 minutes. Next, using the conditions selected above, the optimal conjugate pad positioning was determined (configuration one: mouse IgG-anti-CTX/LT V_HH (conjugate pad containing mouse IgG-AuNP overlapping the nitrocellulose membrane) or configuration two: anti-CTX/LT V_HH-mouse IgG (conjugate pad containing anti-CTX/LT V_HH overlapping the nitrocellulose membrane)). Thereafter, two conjugate pad drying buffers (5 mM borate buffer with 5% or 10% sucrose) were assessed with the optimal conjugate pad positioning (configuration two) using the same experimental conditions.

Using the optimal LFA configuration and conditions selected above, the LFA ($n = 3$) was tested in 5 μL of human fecal sample (sample #1) spiked with CTX-B, LT-B, STX-B, CTX, or LT at concentrations of 0, 0.1, 1, 10, 100, and 1000 ng mL^{-1} or spiked with CTX at concentrations 0, 12.5, 25, 50, and 100 ng mL^{-1}, and 95 μL RB.

2.13. Determining matrix interference in multiple fecal samples

The LFA ($n = 2$) was tested in 11 individual fecal samples spiked with CTX (0, 100, 250, 500, and 1000 ng mL^{-1}) by inserting the LFA into a well containing 5 μL of spiked or blank fecal sample and 95 μL RB and allowing the test to develop for 15 min.

2.14. Detection of cholera toxin in tap water

The LFA ($n = 2$) was first tested in blank or CTX-B spiked (1 ng mL^{-1}) tap water using different sample-to-RB ratios (100 : 0, 50 : 50, and 20 : 80). Thereafter, the LFA was inserted ($n = 2$) into microwells containing 50 μL of tap water spiked with CTX-B (0, 1, 10, 100, and 1000 ng mL^{-1}) and 50 μL RB (PBS with 0.5% BSA and 0.3% Tween-20) and the signal was allowed to develop for 15 min. Blank tap water samples from eight different cities were tested ($n = 2$) using the 50 : 50 sample-to-RB ratio.

2.15. Smartphone-based readout

After 15 minutes, all LFAs were removed from the wells and inserted into a handmade cardboard lightbox (Fig. S1), and a photo was recorded by smartphone (Google Pixel 2XL, Google LLC, USA) using the free OpenCamera app (v.1.51.1). Subsequently, the smartphone images were analyzed using ImageJ[36] as previously described.[28] After splitting the images into their respective red, green, and blue (RGB) color channels, a green channel pixel intensity (GCPI) reading was taken from the test line and from the background below the control line. The green channel was used because it showed the largest pixel-intensity response. The GCPI measurement from the test line was then subtracted from the background to obtain the corrected GCPI (cGCPI). In this work, a cGCPI value above 3 indicates a positive test.

3. Results and discussion

3.1. Identifying optimal conditions and CBM–V_HH pair for rapid toxin detection

The V_HH used in the LFA (anti-CTX/LT V_HH) has been characterized for binding to specific conserved residues of the LT-B/CTX-B GM1 binding pocket.[30,31] CD spectra confirmed the correct folding of the recombinantly expressed proteins (Fig. S2), showing β-sheet-rich structures which is characterized by a positive peak around 195 nm and a negative peak around

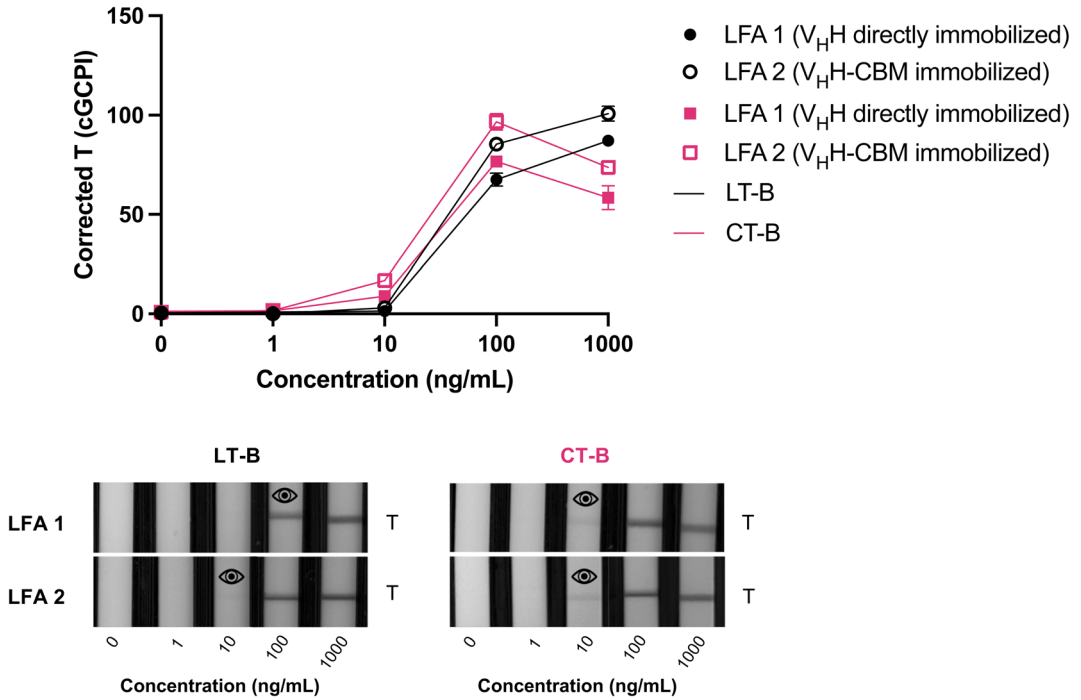

Fig. 2 Calibration curves and smartphone photographs of developed lateral flow assays with single-domain antibodies (V_HHs) directly immobilized at the test line or immobilized using a cellulose-binding module (CBM), tested in duplicate in an increasing concentration range (0–1000 ng mL^{-1}) of cholera toxin B-subunit (CTX-B) in pink or ETEC-LT B-subunit (LT-B) in black, spiked in running buffer. LFA 1 has the V_HH directly immobilized by passive adsorption on the test line, whereas LFA 2 uses a CBM to anchor the V_HH to the test line. Calibration curves are plotted as the corrected green-channel pixel intensity (cGCPI) of the test line against toxin concentration. Error bars display the standard deviation (n = 2) between replicates. T indicates the test line, and the eye icon indicates the lowest concentration that could be visually distinguished from the blank signal by naked eye (*i.e.*, the visual LOD).

215–218 nm, as expected for both V_HHs and CTX-B. Therefore, CTX-B and LT-B were used to spike the RB and evaluate the LFAs. The planned detection scheme is represented in Fig. 1.

To select the most appropriate on-strip conditions for the LFA, several optimizations were carried out. First, the optimal immobilization buffer was evaluated by Ponceau S staining (Fig. S3). A buffer containing 5 mM BB and 1% trehalose resulted in the most intense staining, indicating that more protein was immobilized, as Ponceau staining can detect protein on nitrocellulose membranes.[35] Next, LFAs with test lines consisting of the anti-CTX/LT V_HH fused to either CBM family 1 cel6a (CBM1) or cel7a (CBM2) were compared. These CBMs differ in their binding affinities for cellulose,[32] allowing identification of the most effective CBM for immobilizing the V_HH. The anti-CTX/LT V_HH–CBM1 (2 mg mL^{-1}) fusion improved the assay performance as the test line signal intensities developed on this test were observably more intense at all tested concentrations of CTX-B compared with the signal intensity on the test using an anti-CTX/LT V_HH–CBM2 test line (Fig. S4a & b).

To test the hypothesis that CBMs enhance the immobilization of V_HHs onto (nitro)cellulose membranes, as has previously been reported,[28] an LFA with V_HH directly immobilized at the test line (LFA 1) was compared to an LFA in which the V_HH was immobilized *via* a CBM (LFA 2) fused to the C-terminal (Fig. 2). When tested in RB spiked with either CTX-B or LT-B, the LFA with the bifunctional V_HH–CBM (LFA 2) produced a stronger signal and a sharper test line. This suggests that the CBM enabled more controlled anchoring at the test line. In contrast, V_HHs that were passively adsorbed onto the nitrocellulose membrane resulted in a slightly more diffuse test line, which likely contributed to the reduced signal intensity and could indicate less controlled immobilization. Furthermore, when spiked with LT-B, a lower visual limit of detection (LOD) was observed. Since the concentrations tested were based on 10-fold dilution steps, a lower visual LOD might have been observed for LFA 2 (V_HH–CBM) if tested in RB spiked with CTX-B at smaller concentration intervals (*e.g.*, 2-fold). This indicates that CBM-mediated immobilization improves the anchoring of V_HHs at the test line, either by enhancing V_HH binding to the nitrocellulose membrane or by ensuring optimal immobilization orientation, facilitating target interaction.

Thereafter, the assay RB was optimized by increasing the Tween-20 concentration to facilitate flow and minimize non-specific interactions, with 0.3% producing the most intense test line signal at 10 ng mL^{-1} CTX-B (Fig. S4c).

Before implementing conjugate pads into the test architecture, different volumes of anti-CTX/LT V_HH–AuNP were compared to determine which volume produced the most intense specific signal in spiked RB without introducing false positives in blank RB. Using 4 μL AuNPs yielded the most intense test line signal when tested in a $\frac{1}{2}$-dipstick LFA format (Fig. S4d); therefore, this volume was used to prepare the conjugate pads.

Successful conjugation of V_HH to 40 nm AuNPs (space group $Fm\bar{3}m$, as shown in Fig. S5) was confirmed by ultraviolet-visible spectroscopy (Fig. S6), showing a 4 nm red shift in the localized surface resonance peak (λ_{max} shifted from 523 nm to 527 nm). The maintenance of a sharp, symmetrical peak profile post-conjugation indicates the resulting nanoconjugates remained monodisperse (Fig. S6). Fig. S7 and S8 shows bright-field STEM images of the AuNPs (Fig. S7a), anti-CT/LT-AuNP (Fig. S7b and S8a), and anti-CT/LT-AuNP–V_HH (Fig. S7c and S8b), in which the contrast is mainly defined by mass-thickness properties and, therefore, displays the AuNPs as the darkest feature followed by the protein (or protein plus CTX-B antigen). In Fig. S7a, the AuNP lies on the carbon support film without any clear "deposits" around it, whereas the functionalised AuNPs exhibit a distinct "halo" surrounding the particles. This "halo" was attributed to the anti-CTX/LT V_HH and a mixture of anti-CTX/LT V_HH and antigen (CTX-B), in which the antigen doubled the diameter of this carbonaceous matter surrounding the particle. Another indication that the V_HH functionalization worked is the agglomeration of AuNPs in the presence of CTX-B (Fig. S8b). This could be caused by CTX-B being bound by multiple anti-CTX/LT V_HH–AuNPs simultaneously, leading to agglomeration of the AuNPs.

Moving from a wet $\frac{1}{2}$-dipstick LFA (*i.e.*, without a conjugate or sample pad) to a full-format LFA with AuNPs dried down and pre-stored in a conjugate pad often impacts assay performance and thus requires optimization. Here, three different conjugate pad buffers were compared using a 1 : 1 dilution of the conjugate (anti-CTX/LT V_HH–AuNP) in each buffer. A fourth condition was also compared; this condition used anti-CTX/LT V_HH–AuNP directly on the conjugate pad, without dilution in buffer. It was found that conjugate pads with a 1 : 1 dilution of conjugate in 5 mM BB (pH 8.8) were the most optimal, as these conditions allowed for complete rehydration and release of conjugate from the pad upon wetting (Fig. S4e). Low-concentration buffers, such as BB with stabilizing agents such as sucrose, are typically recommended as conjugate pad buffers, as they ensure long-term stability of the dried-down conjugate while allowing complete rehydration.[39]

The assays were initially optimized using 20% toxin-spiked RB diluted in 80% RB. However, when testing fecal samples, it was determined that 5% (spiked or blank) fecal sample in (95%) RB was the most appropriate for running the assay (Fig. S4f) as it allowed for the most consistent sample flow and for total conjugate pad rehydration, resulting in a clear strip background. However, reducing the sample volume from 20% to 5% also reduced the concentration of antigen available for binding (Table S3); therefore, the reduction of sample volume can be considered a compromise that limits assay sensitivity but improves specificity by limiting matrix effects in fecal samples.

The LFA's test line signal intensities decreased proportionally (resulting in a decreased cGCPI value) to the decreasing concentration of CTX-B or LT-B in the sample, reaching a visual LOD of 1 ng mL^{-1} for CTX-B and 10 ng mL^{-1} for LT-B (absolute concentrations of 0.05 ng mL^{-1} and 0.5 ng mL^{-1}, respectively) when spiked into RB (Fig. 3a).

When spiked into running buffer, a high-antigen-concentration effect (also referred to as the hook effect) can be observed at concentrations above 1000 ng mL^{-1} for CTX-B or LT-B, leading to reduced signal intensity at the test line (Fig. 3a). This occurs when the excess antigen in the sample saturates the

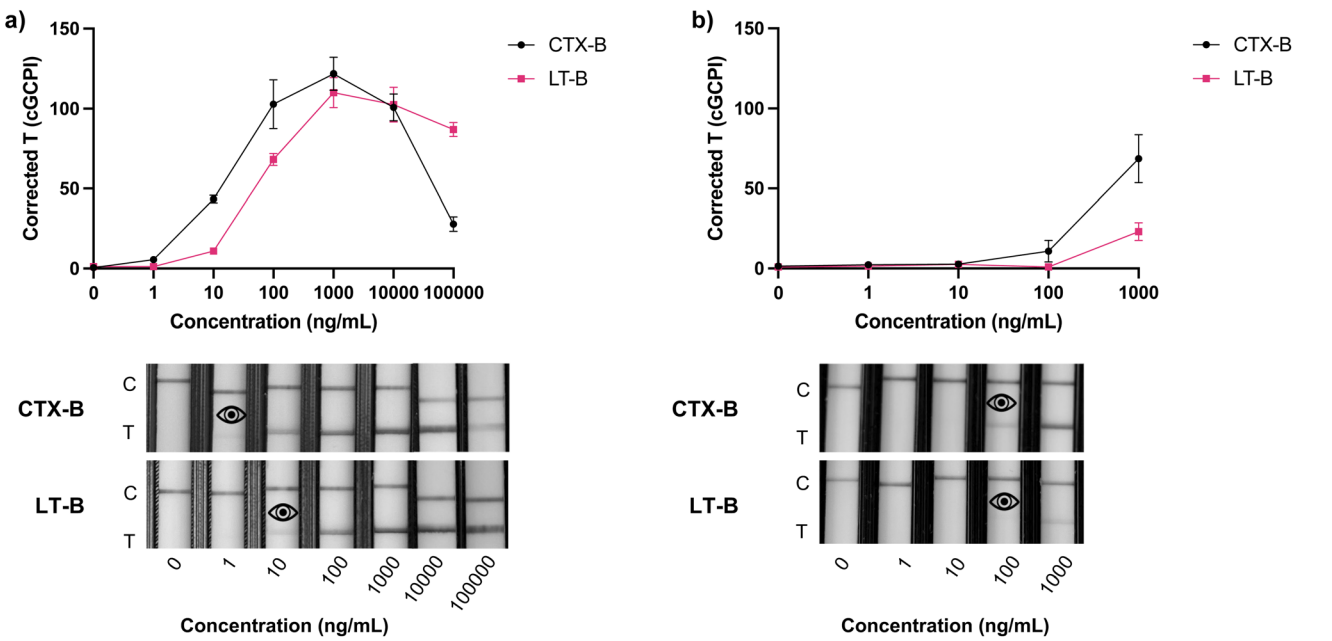

Fig. 3 Calibration curves and smartphone photographs of the developed assay, tested in duplicate in an increasing concentration range of cholera toxin B-subunit (CTX-B) or ETEC-LT B-subunit (LT-B), spiked in (a) running buffer (0–100 000 ng mL^{-1}) or (b) human fecal sample (0–1000 ng mL^{-1}). Calibration curves are plotted as the corrected green channel pixel intensity (cGCPI) of the test line against toxin concentration. Error bars display the standard deviation ($n = 2$) between replicates. C indicates the control line, T indicates the test line and the eye icon indicates the lowest concentration that could be visually distinguished from the blank signal by naked eye (*i.e.*, the visual LOD).

test line, preventing the binding of the anti-CTX/LT V_HH–AuNP at this region and leading to reduced test line signal intensity. At the concentrations tested in this study, there was no complete loss of test line signal, which would be interpreted as a false negative result, however even more extreme concentrations would likely cause this, as previously reported.[40] Although the test line was not completely inhibited, signal intensities (and corresponding cGCPI values) at the highest concentration tested (100 000 ng mL^{-1}) could be misinterpreted as a much lower response. This effect was most pronounced for CTX-B, where the signal at 100 000 ng mL^{-1} was lower than at 10 ng mL^{-1}. In contrast, when tested in LT-B, the LFA did not have such a strong hook effect, likely because 100 000 ng mL^{-1} does not exceed the assay's upper dynamic range for this toxin. Accordingly, higher LT-B concentrations would be required to induce a hook effect, as visually detectable test line signals only emerged at ≥10 ng mL^{-1} (Fig. 3a). In any case, the high concentrations tested in this study exceed those expected in infected patients.[41]

In contrast, a visual LOD of 100 ng mL^{-1} (5 ng mL^{-1}: absolute concentration) was observed for both toxins when spiked into human fecal samples (Fig. 3b), indicating that some matrix interference was affecting signal development. While the sensitivity decreased in the fecal samples, assay specificity remained high, with no false positives or background staining detected (Fig. 3b). Since the overall signal was reduced in fecal samples, it could be expected that any high-antigen-concentration effect impacting the test line would occur at even higher concentrations than those shown for spiked RB in Fig. 3a. While there are no commercial LFAs for the specific detection of only LT, other LFAs have been reported in the literature for the detection of CTX and LT (see Table S1).[42,43] For example, one IgG-based LFA was able to detect CTX and LT at 10 ng mL^{-1} in spiked running buffer,[43] however, as this assay was not assessed in biological or environmental matrices, it is difficult to assess its potential real-life applicability. In another study, researchers reported a proof-of-concept aptamer-based LFA for CTX detection. In this work, both competitive and sandwich-format LFAs were developed, achieving visual LODs of 100 ng mL^{-1} and 1 ng mL^{-1}, respectively. However, in both of these works, the assays were only evaluated in toxin-spiked running buffer, and not in any relevant biological matrix.[42,43] Other researchers have reported extremely sensitive assays, such as the proof of concept liposome PCR that reached an LOD of 10 pg mL^{-1}, however, this is a molecular technique which is more complex and time-consuming than LFAs, which would limit its use case as a point-of-care test outside of a centralised laboratory.[44] In other interesting examples, researchers developed a label-free carbon dots-based fluorescent aptasensor that was able to detect *V. cholerae* with an LOD of 426 CFU mL^{-1},[45] and a loop-mediated isothermal amplification-based assay was able to reach LODs of ~104 CFU g^{-1} of human feces in under one hour.[46] It should be noted that comparing LODs expressed in CFU mL^{-1} and ng mL^{-1} is challenging as they represent different biological measures that are not directly correlated. Still, to have societal impact, LFAs for CTX detection should be able to detect the toxin at approximately 100 ng mL^{-1} in fecal samples[47] or 1 ng mL^{-1} in water samples.[44]

3.2. Lateral flow assay optimization for rapid toxin detection in human fecal samples

Further optimizations were carried out to reach clinically relevant toxin detection levels in human fecal samples. By adding 0.5% BSA to the RB, the test line signal intensity increased in fecal samples spiked with 100 ng mL^{-1} CTX and did not cause any false positive signal in blank samples (Fig. S9a). This increase in intensity is likely because BSA can block non-specific interactions by binding to the fecal components that might interfere with the V_HHs, thereby allowing the sandwich interaction to occur and the signal to develop. In previous work,[28] we identified the challenge in finding an appropriate control line antibody in a different sandwich format, V_HH-based LFA. To circumvent this issue, we tested 0.5 mg mL^{-1} or 1 mg mL^{-1} anti-alpaca IgG as a control line antibody, but this yielded only a very weak control line signal (Fig. S10). As an alternative solution, goat-anti-mouse IgG was immobilized as a control line, and an additional AuNP conjugated to mouse IgG was included, allowing the development of a control line signal when the AuNP-mouse IgG reached the anti-mouse IgG at the control line region. Gold coupling of mouse IgG was confirmed with UV-Vis spectroscopy showing a 4 nm red shift in the localized surface resonance peak (λ_{max} shifted from 523 nm to 527 nm). The inclusion of this additional AuNP conjugate required an extra conjugate pad to be added to the test (see Fig. 1 for the architecture of the LFA).

The conjugate pads were tested in two positions (Fig. S9b), and the LFA with the conjugate containing anti-CTX/LT V_HH–AuNP closest to the nitrocellulose membrane (configuration 2) produced the most intense test line signal (Fig. S9b). Lastly, increasing the sucrose to 10% in the conjugate pad buffer improved the signal intensity at 50 and 100 ng mL^{-1} and resulted in a clearer background (Fig. S9c). This is likely because the increased sucrose both enabled better conjugate stability and slowed down the release of the conjugate upon rehydration, allowing more time for the anti-CTX/LT V_HH–AuNP to form a complex with the toxin in the sample.[47]

These optimizations enabled the assay to reach visual LODs of 10 ng mL^{-1} for CTX-B, 12.5 ng mL^{-1} for CTX, and 100 ng mL^{-1} for LT-B and LT (absolute concentrations of: 0.5 ng mL^{-1}, 0.625 ng mL^{-1}, and 5 ng mL^{-1}, respectively) (Fig. 4). The decrease in sensitivity for CTX compared to CTX-B was anticipated as CTX is one and a half times larger than CTX-B pentamers.[48] The larger antigen could result in steric hindrance, blocking free V_HHs at the test line. Despite the decrease in sensitivity for the detection of the whole toxin, the test is still able to detect a clinically relevant concentration for patients with acute cholera infection, which is around 100 ng mL^{-1}.[41,49,50]

CTX-B and LT-B are structurally and functionally similar.[51] In contrast, the AB_5-type Shiga toxin produced by Shiga toxin-producing *E. coli* (STEC) targets a different receptor (globotriaosylceramide) on kidney and endothelial cells.[52] The LFA

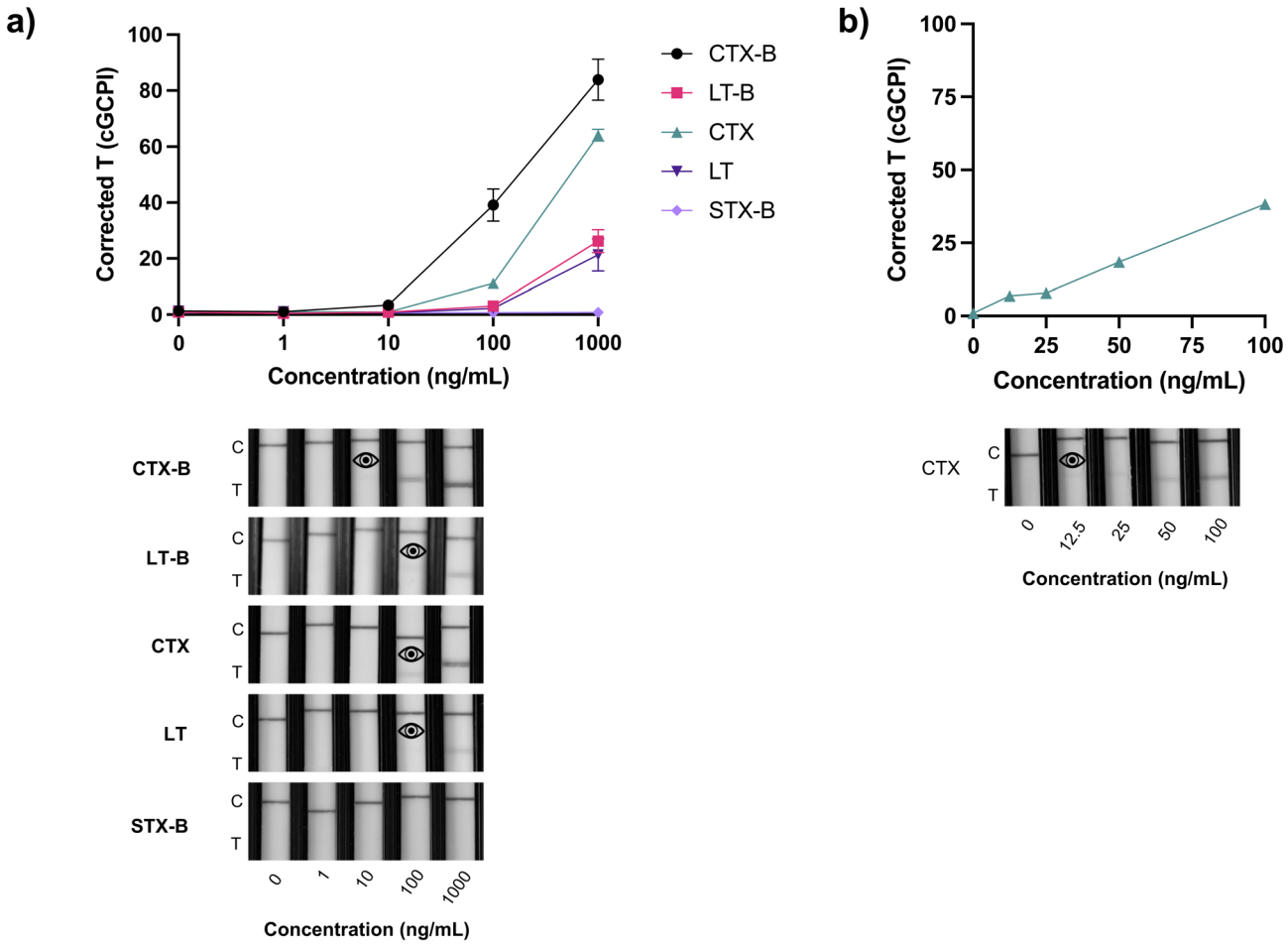

Fig. 4 Calibration curves and smartphone photographs of the assay optimized for fecal samples, tested in triplicate in an increasing concentration range (0–1000 ng mL^{-1}) of (a) cholera toxin B-subunit (CTX-B), cholera toxin (CTX), ETEC-LT B-subunit (LT-B), ETEC-LT (LT), and Shiga toxin B subunit (STX-B) or (b) (0–100 ng mL^{-1}) of CTX spiked in fecal sample. Calibration curves are plotted as the corrected green channel pixel intensity (cGCPI) of the test line against toxin concentration. Error bars display the standard deviation ($n = 3$) between replicates. C indicates the control line, T indicates the test line and the eye icon indicates the lowest concentration that could be visually distinguished from the blank signal by the naked eye (*i.e.*, the visual LOD).

reported in this study can detect both CTX and LT, but not STX (Fig. 4). This is clinically relevant as both cholera and ETEC infections are treated similarly with rehydration and, in some cases, with antibiotics,[1,53] whereas for STEC, supportive care alone is recommended.[54,55] Therefore, this test could reduce the inappropriate use of antibiotics for STEC. In addition, as the anti-CTX/LT V_HH targets an epitope that is conserved among LT toxinotypes relevant to human infection and among all pandemic cholera strains to date,[31,56] we expect that the assay would be able to detect CTX and LT across all relevant serovars.

Differentiating between *V. cholerae* and ETEC remains important, both for treatment decisions and especially for outbreak source tracking. In the clinic, simply ascertaining that a toxigenic bacterium is the causative agent of the disease can support appropriate initiation of antibiotic usage. Today, antibiotics are prescribed based on symptoms alone due to the lack of rapid tests for pathogen identification. Confirming the presence of one of the toxins, and therefore one of the two bacteria, could potentially help reduce the use of antibiotics for viral infections with symptoms that resemble cholera and ETEC, *e.g.*, infections by rotavirus or norovirus. However, the structural similarity between CTX and LT makes it challenging to develop binders that discriminate between these two toxins. Indeed, other assays developed for detecting CTX have also been reported to cross-detect LT.[43] One possible solution to overcome this challenge of cross-detection could be to isolate and use V_HHs that recognize regions of CTX-A or LT-A that are less conserved. However, this may be complicated by the limited sequence conservation within a toxinotype, which could make it challenging to achieve strong and specific binding across all LT or CTX variants. Such V_HHs could potentially be discovered using phage or yeast display selection strategies, including CTX or LT for deselection to ensure that the binder only binds to CTX or LT.[57]

3.3. Determining the LFA's capability of detecting CTX in multiple fecal samples from individual donors

To assess the robustness of the assay in samples from different donors, the LFA was tested in 11 human fecal samples with and

without CTX spiked in. It is well known that fecal composition is highly variable between individuals and is influenced by factors such as diet, ethnicity, age, gut microbiota physiological status, gut transit time, and stool consistency.[58,59]

Among the tested samples, five (#1, 3, 4, 8, 11) produced a test line signal down to 100 ng mL^{-1} (5 ng mL^{-1}: absolute concentration), and three (#5, #6 and #7) down to 1000 ng mL^{-1} (50 ng mL^{-1}: absolute concentration), while the remaining three (#2, #9 and #10) produced no test line at any of the tested concentrations. Furthermore, one sample (#11) produced a false positive signal (*i.e.*, the appearance of a test line in a sample free from the target antigen) (Fig. 5). In this sample (#11), the test line signal at 100 ng mL^{-1} was still higher than the false positive (0 ng mL^{-1}), but the intensity of the test line in the unspiked sample indicates that some interfering component present in this fecal sample was interacting with the V_HHs.

Variability in protein content in fecal samples can affect the detection of target analytes. At the same time, any proteases present in the sample can further degrade proteins and impair downstream analysis.[59] To mimic this variability, the samples tested here were from different individual donors with varying age, gender, ethnicity, weight, height, health conditions, medications, and fecal consistency according to the Bristol Stool Chart (Table S2). Considering the diversity of the donors, it is understandable that the performance of the LFA was considerably impacted by the different samples (Fig. 5).

The large differences in sensitivity across samples demonstrate the challenging nature of detecting toxins in complex samples such as feces. In this work, the assay conditions were initially optimized using a sample from a single donor (#1). As a result of the assay optimizations, sample #1 produced an intense test line signal at all tested concentrations with no false positives. In contrast, a weaker test line signal intensity was obtained when testing some of the samples from other donors. In future work, to address this variability, additional sample preparation would likely be required to minimize interference from the feces and to ensure effective interaction between the immunoreagents and the toxin, although standard extraction protocols optimized for single samples may be difficult to generalize.[59]

Measuring one specific protein in the complex mixture of proteins present in fecal matter poses challenges.[59] In fact, fecal matter is a highly heterogeneous biological matrix composed of enzymes, bile salts, undigested food particles, microorganisms, and metabolic by-products, which complicates the access to intact proteins for reliable detection by immunoassays.[59] Furthermore, it is documented that the presence of bile salts can impact protein structure and conformation across both V_HH and protein target, complicating reliable and uniform detection.[60] For protein extraction, mechanical disruption of the fecal sample is essential to break insoluble particulates and bacterial cell walls, facilitating protein release. In this study, an additional vortexing step (30 seconds) was added before adding the sample to the LFA to ensure proper protein release.[59] Therefore, developing diagnostic tools for complex variable matrices, such as human fecal samples, requires substantial work to develop a universal extraction method, with the caveat that sample preparation should not detract from the usability (or affordability) of the test.

The fecal samples tested in this study were from healthy donors, ranging from 1 to 6 on the Bristol Stool Chart[61] (Table S2). To mimic the consistency of diarrhea samples (Bristol Stool Chart = 7), the fecal samples were diluted 1 : 1 in water before spiking and testing. A 1 : 1 dilution was selected as it allowed for a more liquid sample without substantially diluting the other potential interferents present in the sample. However, as fecal

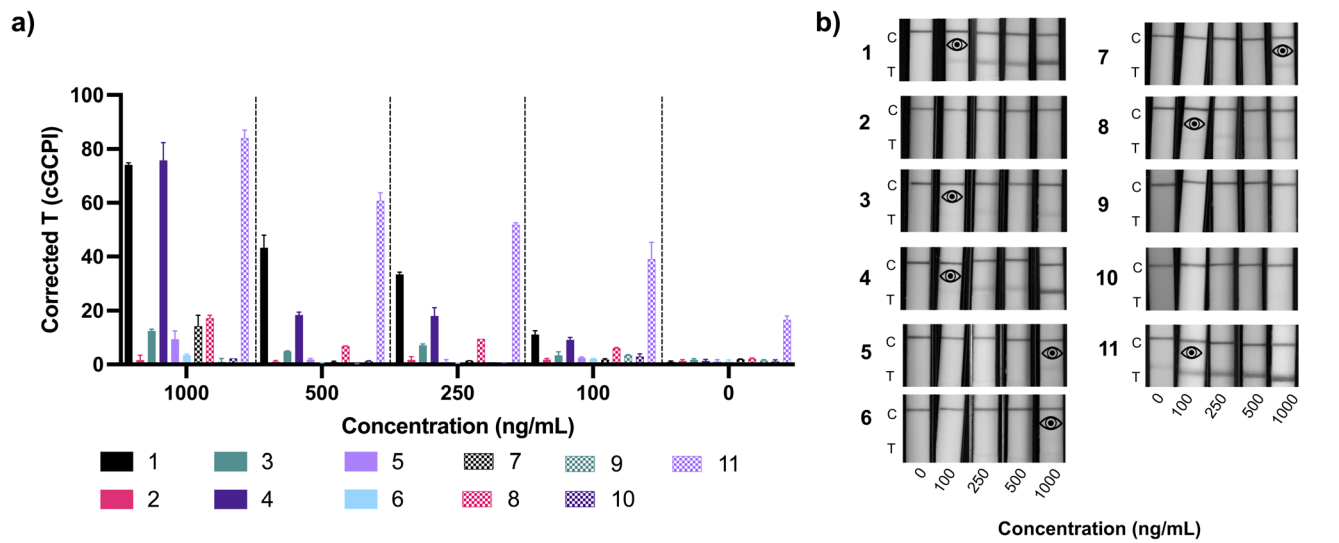

Fig. 5 (a) Graph and (b) smartphone photographs of the lateral flow assay (LFA) tested in duplicates in increasing concentrations (0, 100, 250, 500, and 1000 ng mL^{-1}) of cholera toxin (CTX) spiked into eleven different fecal samples. The graph depicts the corrected green channel pixel intensity (cGCPI) of the test line against sample number. Error bars display the standard deviation ($n = 2$) between replicates. C indicates the control line, T indicates the test line, and the eye icon indicates the lowest concentration that could be visually distinguished from the blank signal by the naked eye (*i.e.*, the visual LOD).

samples from cholera and ETEC patients are characterized by their "rice water" appearance,[62] it is hypothesized that real-life samples would be more fluid than was achieved here using a 1 : 1 dilution. Indeed, the commercially available cholera LFAs rely on liquid stool, which can be added to the sample pad using a disposable pipette or rectal swab samples,[16] highlighting the complexity of using "normal" solid stool (Bristol Stool Chart = 3–4) for testing. For future development, processing a rectal swab for LFA analysis could be considered if the test's sensitivity permits.

3.4. Detection of toxins in environmental samples

V. cholerae and ETEC can spread through contaminated water, making their detection in water samples relevant for indicating environmental presence during an outbreak. In wastewater and other environmental surveillance, detecting the toxin rather than the bacterium can indicate merging or ongoing outbreaks and continued water contamination by human fecal material. If sensitive enough, a test detecting the toxin would be particularly relevant, as it distinguishes toxigenic strains with clinical risk from non-toxigenic environmental strains, like the one recently found in Copenhagen sewage using genomics.[11] Furthermore, due to substantial dilution in environmental waters, it is anticipated that toxin concentrations will be very low as they will originate from fecal contamination, which could present challenges for detection.

Another use case of the test could be the detection of ETEC in environmental samples from pig farms, where it is documented that ETEC causes post-weaning diarrhea in piglets.[63] Here, swab samples could be taken from different pen surfaces, fecal samples from the pigs, or water samples from the troughs. To assess the sensitivity of the assay if used to detect CTX in contaminated water sources, CTX-B was spiked into (tap) water. In contrast to fecal samples, water does not require such a substantial dilution into RB to flow up the strip. Three different sample-to-RB ratios were tested, 100 : 0, 50 : 50, and 20 : 80, with a 50 : 50 ratio resulting in the best flow and the most intense signal at 1 ng mL^{-1} (Fig. S11).

The assay was able to reach an LOD of 1 ng mL^{-1} (0.5 ng mL^{-1}: absolute concentration) of CTX-B when spiked into water (Fig. 6). That is comparable to, or even an improvement over, the standard optical ELISA (1 ng mL^{-1}) or a magnetic bead-based sandwich enzyme-linked aptamer assay in tap water (2.4 ng mL^{-1}), while providing a more rapid and user-friendly alternative with fewer analytical steps.[44] Furthermore, no false positive signals developed in blank tap water samples from eight different cities (Fig. S12). Moreover, it is expected that this LOD could be further improved by using a 100 : 0 sample-to-RB ratio. However, to ensure enough Tween-20 for an appropriate flow, Tween-20 should be added to the sample or conjugate pad.

Still, environmental testing alone cannot confirm active disease outbreaks and must be complemented with fecal testing from symptomatic patients.[64] The ability of the presented test to function in both fecal and water samples is therefore particularly valuable. Environmental monitoring of water sources remains important, as identifying contaminated sources can guide outbreak control through source removal. However, for assessing if water has fecal contamination or is safe to drink, *V. cholerae* detection should be combined with standard fecal contamination indicators such as crAssphage,[65] thermotolerant coliforms, *Escherichia coli*, and fecal *streptococci*.[64] In the context of environmental water monitoring, LFAs are suitable screening tools that can be applied to sort samples requiring confirmatory testing in a reference laboratory, thereby reducing the overall number of samples that need to be tested by these more complex, expensive, and time-consuming methods.

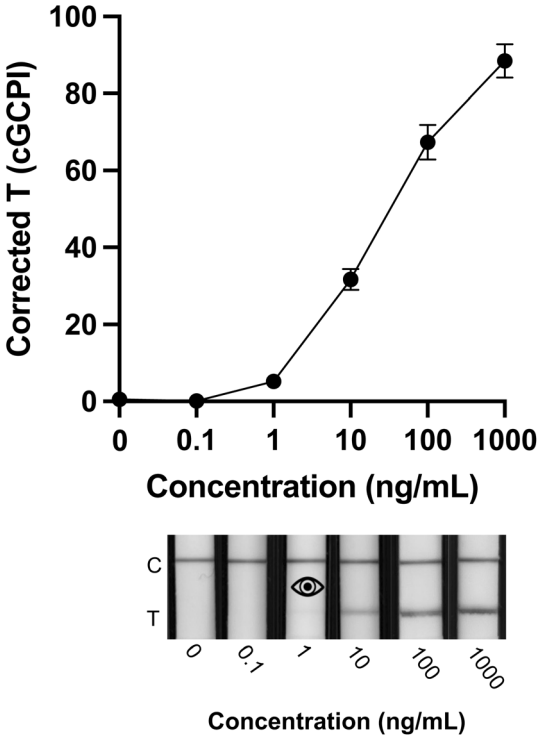

Fig. 6 Calibration curves and smartphone photographs of the assay tested in duplicates in an increasing concentration range (0–1000 ng mL^{-1}) of cholera toxin B-subunit (CTX-B) spiked in tap water. Calibration curves are plotted as the corrected green channel pixel intensity (cGCPI) of the test line against CTX-B concentration. Error bars display the standard deviation (n = 2) between replicates. C indicates the control line, T indicates the test line, and the eye icon indicates the lowest concentration that could be visually distinguished from the blank signal by the naked eye (*i.e.*, the visual LOD).

4. Conclusions

Diarrheal diseases caused by *V. cholerae* and ETEC infections, remain a burden in large regions of the world where they continue to be endemic with seasonal epidemic outbreaks. This highlights the importance of developing more accessible diagnostic tools for the early detection of the causative agents of these diseases to limit spread and improve patient and animal care for improved environmental and clinical practices. In this work, we have developed an LFA for the detection of CTX and LT in fecal samples and environmental water samples. The LFA reached an LOD of 12.5 ng mL^{-1} in fecal samples and 1 ng mL^{-1}

in water samples. Although the developed test did not show substantial improvements compared to full-length antibody-based assays, further optimization could enable lower detection limits. In this research, we demonstrated that using CBM to immobilize V_HH onto LFAs can allow the detection of CTX and LT, highlighting a promising approach for future diagnostics using recombinant antibody formats. Moreover, this strategy opens opportunities for companion diagnostics, ensuring that detected antigens can be targeted with the corresponding soluble V_HH.

We exemplify how the simultaneous detection of CTX and LT with the same LFA is feasible, with high sensitivity, and can be relevant due to the similarity in spread, disease manifestation, and clinical management. Nevertheless, distinguishing between the two toxins remains important for future outbreak source tracking.

Fecal samples represent a highly complex biological matrix that poses significant challenges for reliable performance in LFAs. Due to fecal inter-sample variability, it was necessary to use a sample-to-RB ratio of 5 : 95 (μL), reducing the amount of antigen for detection and thereby the overall sensitivity of the assay. Current assays utilize fecal swabs or liquid samples, which may contain less particulate matter, making them easier to process and potentially allowing a higher sample-to-RB ratio. Furthermore, given the variability of fecal samples, testing real samples from target patient groups is essential to determine optimal assay conditions, as differences in ethnicity, diet, and microbiota may affect performance.

The results presented here showcase an opportunity to aid early detection of CTX and LT for clinical and water testing. Such a test could help ease the burden on physicians by providing a rapid, accurate tool for detecting CTX and LT, thereby saving time and costs associated with cholera and ETEC detection.

Author contributions

Conceptualization: S. B. B., J. A. J., S. W. T., A. H. L., G. M. S. R.; data curation: S. B. B., S. T., M. G. M.; formal analysis: S. B. B., M. G. M.; funding acquisition: S. B. B., J. A. J., P. M., A. H. L., G. M. S. R.; investigation: S. B. B., G. M. S. R.; methodology: S. B. B., G. M. S. R.; project administration: S. B. B., J. A. J., S. W. T., G. M. S. R.; resources: J. A. J., S. W. T., A. L., A. H. L., G. M. S. R., supervision: J. A. J., P. M., S. W. T., A. L., A. H. L., G. M. S. R.; validation: S. B. B.; visualization: S. B. B.; writing – original draft: S. B. B., J. A. J., M. P., M. S. W., P. M., A. H. L., G. M. S. R.; writing – review and editing: S. B. B., J. A. J., M. P., M. S. W., P. M., S. W. T., A. L., A. H. L., G. M. S. R.

Conflicts of interest

Laustsen A. H., and Jürgensen J. A. are co-founders of and shareholders in VenomAid Diagnostics ApS. Belfakir S. B., and Ross G. M. S. are employed in VenomAid Diagnostics ApS. Laustsen A. H., and Thrane S. W. are co-founders of and shareholders in Bactolife A/S., and Wraae M. S., are employed in Bactolife A/S. The other author declares no conflict of interest.

Data availability

The data supporting this article have been included as part of the manuscript and the supplementary information (SI). Supplementary information is available. See DOI: https://doi.org/10.1039/d6ra01063f.

Acknowledgements

This project received funding from Innovation Fund Denmark, project number 2052-00023B. P. M. was supported by the Novo Nordisk Foundation (NNF24SA0094147). A. H. L. is supported by a grant from Wellcome (221702/Z/20/Z). S. T. is supported by a scholarship from the Anandamahidol Foundation under the Royal Patronage of His Majesty King Bhumibol Adulyadej of Thailand.

References

1 J. B. Harris, R. C. LaRocque, F. Qadri, E. T. Ryan and S. B. Calderwood, Cholera, *Lancet*, 2012, **379**(9835), 2466–2476, DOI: 10.1016/S0140-6736(12)60436-X.

2 M. Ali, A. R. Nelson, A. L. Lopez and D. A. Sack, Updated Global Burden of Cholera in Endemic Countries, *PLoS Neglected Trop. Dis.*, 2015, **9**(6), e0003832, DOI: 10.1371/journal.pntd.0003832.

3 C. F. Lanata, C. L. Fischer-Walker, A. C. Olascoaga, C. X. Torres, M. J. Aryee and R. E. Black, Global Causes of Diarrheal Disease Mortality in Children <5 Years of Age: A Systematic Review, *PLoS One*, 2013, **8**(9), e72788, DOI: 10.1371/journal.pone.0072788.

4 World Health Organization, *WHO Preferred Product Characteristics for Vaccines against Enterotoxigenic Escherichia Coli*, Report.

5 J. D. Clements and R. A. Finkelstein, Immunological Cross-Reactivity Between a Heat-Labile Enterotoxin(s) of *Escherichia coli* and Subunits of *Vibrio cholerae* Enterotoxin, *Infect. Immun.*, 1978, **21**(3), 1036–1039, DOI: 10.1128/iai.21.3.1036-1039.1978.

6 J. M. Fleckenstein, Confronting Challenges to *Enterotoxigenic Escherichia* coli Vaccine Development, *Front.Trop. Dis.*, 2021, **14**, 2, DOI: 10.3389/fitd.2021.709907.

7 F. Chowdhury, A. G. Ross, M. T. Islam, N. A. J. McMillan and F. Qadri, Diagnosis, Management, and Future Control of Cholera, *Clin. Microbiol. Rev.*, 2022, **35**(3), 1–23, DOI: 10.1128/cmr.00211-21.

8 K. L. Kotloff, J. P. Nataro, W. C. Blackwelder, D. Nasrin, T. H. Farag, S. Panchalingam, *et al.*, Burden and aetiology of diarrhoeal disease in infants and young children in developing countries (the global enteric multicenter study, GEMS): a prospective, case-control study, *Lancet*, 2013, **382**(9888), 209–222, DOI: 10.1016/S0140-6736(13)60844-2.

9 E. J. Nelson, J. A. Grembi, D. L. Chao, J. R. Andrews, L. Alexandrova, P. H. Rodriguez, *et al.*, Gold Standard Cholera Diagnostics Are Tarnished by Lytic Bacteriophage and Antibiotics, *J. Clin. Microbiol.*, 2020, **58**(9), 1–8, DOI: 10.1128/JCM.00412-20.

10 A. M. Smith, K. H. Keddy, H. Ismail, N. Tau, A. Sooka, B. N. Archer, *et al.*, Possible Laboratory Contamination Leads to Incorrect Reporting of *Vibrio cholerae* O1 and Initiates an Outbreak Response, *J. Clin. Microbiol.*, 2012, **50**(2), 480–482, DOI: 10.1128/JCM.05785-11.

11 C. Brinch, S. Otani, P. Munk, M. van den Beld, E. Franz and F. M. Aarestrup, Discovery of *Vibrio cholerae* in Urban Sewage in Copenhagen, Denmark, *Microb. Ecol.*, 2024, **87**(1), 102, DOI: 10.1007/s00248-024-02419-7.

12 G. Chowdhury, D. Ghosh, Y. Zhou, A. K. Deb, A. K. Mukhopadhyay, S. Dutta, *et al.*, Field evaluation of a simple and rapid diagnostic test, RLDT to detect *Shigella* and enterotoxigenic *E. coli* in Indian children, *Sci. Rep.*, 2024, **14**(1), 8816, DOI: 10.1038/s41598-024-59181-6.

13 S. Chakraborty, S. Connor and M. Velagic, Development of a simple, rapid, and sensitive diagnostic assay for enterotoxigenic *E. coli* and *Shigella* spp applicable to endemic countries, *PLoS Neglected Trop. Dis.*, 2022, **16**(1), e0010180, DOI: 10.1371/journal.pntd.0010180.

14 Find, *FIND|Target Product Profile for a Rapid Diagnostic Test for Surveillance of Cholera*, 2024. Report.

15 K. J. Land, D. I. Boeras, X. S. Chen, A. R. Ramsay and R. W. Peeling, REASSURED diagnostics to inform disease control strategies, strengthen health systems and improve patient outcomes, *Nat. Microbiol.*, 2018, **4**(1), 46–54, DOI: 10.1038/s41564-018-0295-3.

16 MdA. Sayeed, K. Islam, M. Hossain, N. J. Akter, MdN. Alam, N. Sultana, *et al.*, Development of a new dipstick (Cholkit) for rapid detection of *Vibrio cholerae* O1 in acute watery diarrheal stools, *PLoS Neglected Trop. Dis.*, 2018, **12**(3), e0006286, DOI: 10.1371/journal.pntd.0006286.

17 P. Kalluri, A. Naheed, S. Rahman, M. Ansaruzzaman, A. S. G. Faruque, M. Bird, *et al.*, Evaluation of three rapid diagnostic tests for cholera: does the skill level of the technician matter?, *Trop. Med. Int. Health*, 2006, **11**(1), 49–55, DOI: 10.1111/j.1365-3156.2005.01539.x.

18 F. Qadri, J. A. Hasan, J. Hossain, A. Chowdhury, Y. A. Begum, T. Azim, *et al.*, Evaluation of the monoclonal antibody-based kit Bengal SMART for rapid detection of *Vibrio cholerae* O139 synonym Bengal in stool samples, *J. Clin. Microbiol.*, 1995, **33**(3), 732–734, DOI: 10.1128/jcm.33.3.732-734.1995.

19 E. Baranova, Development of lateral flow test for the fast identification of *Vibrio Cholerae* O1, *Int. J. Infect. Dis.*, 2012, **16**, e122, DOI: 10.1016/j.ijid.2012.05.278.

20 J. Mwaba, E. Ferreras, E. Chizema-Kawesa, D. Mwimbe, F. Tafirenyika, J. Rauzier, *et al.*, Evaluation of the SD bioline cholera rapid diagnostic test during the 2016 cholera outbreak in Lusaka, Zambia, *Trop. Med. Int. Health*, 2018, **23**(8), 834–840, DOI: 10.1111/tmi.13084.

21 J. Hu, S. Wang, L. Wang, F. Li, B. Pingguan-Murphy, T. J. Lu, *et al.*, Advances in paper-based point-of-care diagnostics, *Biosens. Bioelectron.*, 2014, **54**, 585–597, DOI: 10.1016/j.bios.2013.10.075.

22 V. Shirshahi and G. Liu, Enhancing the analytical performance of paper lateral flow assays: From chemistry to engineering, *TrAC, Trends Anal. Chem.*, 2021, **136**, 116200, DOI: 10.1016/j.trac.2021.116200.

23 Y. Wang, R. Luo, H. Yang, P. Liu, Y. Zhang, S. Dong, *et al.*, Minimalist nanobody architecture: A double-edged sword for immunological analysis, *TrAC, Trends Anal. Chem.*, 2025, **192**, 118382, DOI: 10.1016/j.trac.2025.118382.

24 B. K. Jin, S. Odongo, M. Radwanska and S. Magez, NANOBODIES®: A Review of Diagnostic and Therapeutic Applications, *Int. J. Mol. Sci.*, 2023, **24**(6), 5994, DOI: 10.3390/ijms24065994.

25 T. A. Bates, S. K. Gurmessa, J. B. Reyes-Weinstein, E. Barklis and F. G. Tafesse, A Nanobody-Based Lateral Flow Assay for Point-of-Care Diagnostics, *Biosensors*, 2026, **16**(2), 132, DOI: 10.3390/bios16020132.

26 T. Gong, W. Shen, K. Chen, M. Bi, C. Liu, H. Zheng, *et al.*, Nanoparticle-free dualmodal lateral flow immunoassay for sensitive detection of aflatoxin B1 based on "four-in-one" multifunctional nanobody, *Anal. Chim. Acta*, 2026, **1386**, 345013, DOI: 10.1016/j.aca.2025.345013.

27 N. R. Kang, J. Im, J. R. Biondo, C. E. Sharpes, K. A. Rhea, P. M. Garden, *et al.*, A Rapid and Modular Nanobody Assay for Plug-and-Play Antigen Detection, *ACS Synth. Biol.*, 2025, **14**(9), 3423–3433, DOI: 10.1021/acssynbio.5c00182.

28 S. B. Belfakir, E. R. Rodriguez-Rodriguez, S. W. Thrane, A. Ljungars, W. E. Svendsen, A. H. Laustsen, *et al.*, Leveraging cellulose-binding domains to orient and immobilize single-domain antibodies onto paper-based immunoassays, *Sens. Actuators, B*, 2025, **439**, 137833, DOI: 10.1016/j.snb.2025.137833.

29 A. Elter, T. Bock, D. Spiehl, G. Russo, S. C. Hinz, S. Bitsch, *et al.*, Carbohydrate binding module-fused antibodies improve the performance of cellulose-based lateral flow immunoassays, *Sci. Rep.*, 2021, **11**(1), 7880, DOI: 10.1038/s41598-021-87072-7.

30 M. M. Harmsen, C. B. van Solt and H. P. D. Fijten, Enhancement of toxin- and virus-neutralizing capacity of single-domain antibody fragments by N-glycosylation, *Appl. Microbiol. Biotechnol.*, 2009, **84**(6), 1087–1094, DOI: 10.1007/s00253-009-2029-1.

31 M. Petersson, J. S. Pettersen, H. Bay Pedersen, Á. Duzs, M. L. Fernández-Quintero, N. J. Burlet, *et al.*, Attenuating ETEC virulence using a heat-labile enterotoxin–blocking binding protein, *Gut Microbes*, 2026, **18**(1), 2597567, DOI: 10.1080/19490976.2025.2597567.

32 J. Guo and J. M. Catchmark, Binding Specificity and Thermodynamics of Cellulose-Binding Modules from Trichoderma reesei Cel7A and Cel6A, *Biomacromolecules*, 2013, **14**(5), 1268–1277, DOI: 10.1021/bm300810t.

33 C. Rimbault, P. D. Knudsen, A. Damsbo, K. Boddum, H. Ali, C. M. Hackney, *et al.*, A single-chain variable fragment selected against a conformational epitope of a recombinantly produced snake toxin using phage display, *New Biotechnol.*, 2023, **76**, 23–32, DOI: 10.1016/j.nbt.2023.04.002.

34 K. Tripathi and J. D. Driskell, Quantifying Bound and Active Antibodies Conjugated to Gold Nanoparticles: A Comprehensive and Robust Approach To Evaluate Immobilization Chemistry, *ACS Omega*, 2018, **3**(7), 8253–8259, DOI: 10.1021/acsomega.8b00591.

35 H. Sander, S. Wallace, R. Plouse, S. Tiwari and A. V. Gomes, Ponceau S waste: Ponceau S staining for total protein normalization, *Anal. Biochem.*, 2019, **575**, 44–53, DOI: 10.1016/j.ab.2019.03.010.

36 C. A. Schneider, W. S. Rasband and K. W. Eliceiri, NIH Image to ImageJ: 25 years of image analysis, *Nat. Methods*, 2012, **9**(7), 671–675, DOI: 10.1038/nmeth.2089.

37 T. K. Sixma and W. G. J. Hol, *Refined Structure of E. coli Heat Labile Enterotoxin, a Close Relative of Cholera Toxin*, Worldwide Protein Data Bank, 1994, DOI: 10.2210/pdb1lts/pdb.

38 R. G. Zhang and E. Westbrook, *Cholera Toxin*, Worldwide Protein Data Bank, 1996, DOI: 10.2210/pdb1xtc/pdb.

39 NanoComposix. *Conjugate Pad Selection, Treatment, and Conjugate Drying for Lateral Flow Assays*.

40 G. M. S. Ross, D. Filippini, M. W. F. Nielen and G. I. J. Salentijn, Unraveling the Hook Effect: A Comprehensive Study of High Antigen Concentration Effects in Sandwich Lateral Flow Immunoassays, *Anal. Chem.*, 2020, **92**(23), 15587–15595, DOI: 10.1021/acs.analchem.0c03740.

41 T. Ramamurthy, S. K. Bhattacharya, Y. Uesaka, K. Horigome, M. Paul, D. Sen, *et al.*, Evaluation of the bead enzyme-linked immunosorbent assay for detection of cholera toxin directly from stool specimens, *J. Clin. Microbiol.*, 1992, **30**(7), 1783–1786, DOI: 10.1128/jcm.30.7.1783-1786.1992.

42 E. Frohnmeyer, N. Tuschel, T. Sitz, C. Hermann, G. T. Dahl, F. Schulz, *et al.*, Aptamer lateral flow assays for rapid and sensitive detection of cholera toxin, *Analyst*, 2019, **144**(5), 1840–1849, DOI: 10.1039/C8AN01616J.

43 H. Arimitsu, K. Sasaki and T. Tsuji, Immunochromatographic detection of the heat-labile enterotoxin of enterotoxigenic Escherichia coli with cross-detection of cholera toxin, *J. Microbiol. Methods*, 2017, **132**, 148–152, DOI: 10.1016/j.mimet.2016.12.007.

44 E. Frohnmeyer, F. Frisch, S. Falke, C. Betzel and M. Fischer, Highly affine and selective aptamers against cholera toxin as capture elements in magnetic bead-based sandwich ELAA, *J. Biotechnol.*, 2018, **269**, 35–42, DOI: 10.1016/j.jbiotec.2018.01.012.

45 M. Karthikeyan, G. D. Venkatasubbu and P. Rathinasabapathi, A label-free carbon dots-based fluorescent aptasensor for the detection of V. cholerae O139, *Diamond Relat. Mater.*, 2023, **137**, 110173, DOI: 10.1016/j.diamond.2023.110173.

46 S. Chakraborty, M. Velagic and S. Connor, Development of a simple, rapid, and sensitive molecular diagnostic assay for cholera, *PLoS Neglected Trop. Dis.*, 2023, **17**(2), e0011113, DOI: 10.1371/journal.pntd.0011113.

47 C. Parolo, A. Sena-Torralba, J. F. Bergua, E. Calucho, C. Fuentes-Chust, L. Hu, *et al.*, Tutorial: design and fabrication of nanoparticle-based lateral-flow immunoassays, *Nat. Protoc.*, 2020, **15**(12), 3788–3816, DOI: 10.1038/s41596-020-0357-x.

48 J. J. Mekalanos, D. J. Swartz, G. D. N. Pearson, N. Harford, F. Groyne and M. de Wilde, Cholera toxin genes: nucleotide sequence, deletion analysis and vaccine development, *Nature*, 1983, **306**(5943), 551–557, DOI: 10.1038/306551a0.

49 K. M. S. Aziz and W. H. Mosley, Quantitative Studies of Toxin in the Stools and Jejunal Aspirates of Patients with Cholera, *J. Infect. Dis.*, 1972, **125**(1), 36–44, DOI: 10.1093/infdis/125.1.36.

50 P. Varela, G. D. Pollevick, M. Rivas, I. Chinen, N. Binsztein, A. C. Frasch, *et al.*, Direct detection of *Vibrio cholerae* in stool samples, *J. Clin. Microbiol.*, 1994, **32**(5), 1246–1248, DOI: 10.1128/jcm.32.5.1246-1248.1994.

51 W. S. Dallas and S. Falkow, Amino acid sequence homology between cholera toxin and *Escherichia coli* heat-labile toxin, *Nature*, 1980, **288**(5790), 499–501, DOI: 10.1038/288499a0.

52 P. I. Brown, A. Ojiakor, A. J. Chemello and C. C. Fowler, The diverse landscape of AB5-type toxins, *Eng. Microbiol.*, 2023, **3**(4), 100104, DOI: 10.1016/j.engmic.2023.100104.

53 F. Qadri, A. M. Svennerholm, A. S. G. Faruque and R. B. Sack, Enterotoxigenic *Escherichia coli* in Developing Countries: Epidemiology, Microbiology, Clinical Features, Treatment, and Prevention, *Clin. Microbiol. Rev.*, 2005, **18**(3), 465–483, DOI: 10.1128/CMR.18.3.465-483.2005.

54 S. Mühlen and P. Dersch, Treatment Strategies for Infections With Shiga Toxin-Producing *Escherichia coli*, *Front. Cell. Infect. Microbiol.*, 2020, **10**(169), 1–17, DOI: 10.3389/fcimb.2020.00169.

55 P. I. Tarr and S. B. Freedman, Why antibiotics should not be used to treat Shiga toxin-producing *Escherichia coli* infections, *Curr. Opin. Gastroenterol.*, 2022, **38**(1), 30–38, DOI: 10.1097/MOG.0000000000000798.

56 E. J. Kim, C. H. Lee, G. B. Nair and D. W. Kim, Whole-genome sequence comparisons reveal the evolution of *Vibrio cholerae* O1, *Trends Microbiol.*, 2015, **23**(8), 479–489, DOI: 10.1016/j.tim.2015.03.010.

57 L. Ledsgaard, A. Ljungars, C. Rimbault, C. V. Sørensen, T. Tulika, J. Wade, *et al.*, Advances in antibody phage display technology, *Drug Discovery Today*, 2022, **27**(8), 2151–2169, DOI: 10.1016/j.drudis.2022.05.002.

58 K. Kruger, Y. Myeonghyun, N. van der Wielen, D. E. Kok, G. J. Hooiveld, S. Keshtkar, *et al.*, Evaluation of inter- and intra-variability in gut health markers in healthy adults using an optimised faecal sampling and processing method, *Sci. Rep.*, 2024, **14**(1), 24580, DOI: 10.1038/s41598-024-75477-z.

59 S. B. S. Devan, R. Ramli, S. A. Alshehade, S. Y. M. Lim and N. Mamat, Comparison of the techniques for isolating immunoassay-suitable proteins from heterogeneous fecal samples, *Anal. Biochem.*, 2025, **698**, 115748, DOI: 10.1016/j.ab.2024.115748.

60 E. R. Rodriguez Rodriguez, R. T. Nordvang, M. Petersson, J. K. H. Rendsvig, E. W. Arendrup, M. L. Fernández Quintero, *et al.*, Fit-for-purpose heterodivalent single-domain antibody for gastrointestinal targeting of toxin B from *Clostridium difficile*, *Protein Sci.*, 2024, **33**(7), 1–19, DOI: 10.1002/pro.5035.

61 S. J. Lewis and K. W. Heaton, Stool Form Scale as a Useful Guide to Intestinal Transit Time, *Scand. J. Gastroenterol.*, 1997, **32**(9), 920–924, DOI: 10.3109/00365529709011203.

62 L. C. Alexakis, Cholera -"Rice water stools.", *Pan Afr. Med. J.*, 2017, **26**, 147, DOI: 10.11604/pamj.2017.26.147.11874.
63 M. P. Rydal, K. K. Lyderik, A. B. Andersen, C. B. Jørgensen, P. Damborg and J. P. Nielsen, Outbreaks of post-weaning diarrhea caused by ETEC F4 are strongly associated with CHCF1 genotype in Danish pigs, *Sci. Rep.*, 2025, **15**(1), 41748, DOI: 10.1038/s41598-025-26829-w.
64 Global Task Force on Cholera Control S laboratory working group/wash working group, *Technical Note Environmental Surveillance for Cholera Control*, 2022 Oct. Report.
65 M. A. Sabar, R. Honda and E. Haramoto, CrAssphage as an indicator of human-fecal contamination in water environment and virus reduction in wastewater treatment, *Water Res.*, 2022, **221**, 118827, DOI: 10.1016/j.watres.2022.118827.